Formulae for calculating elastic buckling loads for web crippling of rectangular hollow sections

R. Dai, L. Gardner, M.A. Wadee
Department of Civil and Environmental Engineering
Imperial College London, London, United Kingdom

ABSTRACT: Formulae for determining the elastic buckling loads of structural steel rectangular hollow sections (RHS) subjected to concentrated transverse forces are presented herein. The predicted elastic buckling load is bounded by a theoretical lower bound, where only the material within the bearing length is mobilised, and a practical upper bound, where the adjacent material is mobilised to its maximum extent. The lower bound is the elastic buckling load of a wide plate with a width equal to the bearing length and a length equal to the web depth, while the upper bound is determined from finite element (FE) analyses of various representative loading scenarios. The level of mobilisation of adjacent material (i.e., where a specific case lies between the lower and upper bounds) is quantified by introducing a coefficient ζ that is calibrated through FE analyses in the commercial package ABAQUS. The rotational stiffness afforded to the webs by the flanges is also captured. The four loading scenarios defined in the North American Specification (NAS) and Australian/New Zealand Standard (AS/NZS) for the design of cold-formed steel structures, namely the Interior-Two-Flange (ITF), End-Two-Flange (ETF), Interior-One-Flange (IOF) and End-One-Flange (EOF) loading conditions, alongside their transitional cases, are considered. Rectangular hollow sections with a broad spectrum of cross-sectional geometric proportions and bearing lengths encompassing the aforementioned loading conditions are considered. It is found that the developed formulae for predicting the elastic buckling loads under concentrated transverse forces provide accurate results that are typically within 5% of the numerical values. Hence, the developed formulae can be employed as a convenient alternative to numerical methods in advanced structural design methodologies, such as the Direct Strength Method (DSM) and the Continuous Strength Method (CSM).

1 INTRODUCTION

Cold-formed structural steel members under concentrated transverse loads are known to be susceptible to web crippling failure, particularly if the influenced region is unstiffened. Stiffening of tubular members, such as rectangular hollow section (RHS) and square hollow section (SHS) members, is often inconvenient and uneconomical (Li & Young 2018). Hence, these sections are particularly vulnerable to web crippling failure and thus require suitable design provisions.

Investigations into web crippling have been conducted by researchers since the 1940s for various cross-section types and loading conditions. Most of these investigations have focused on open sections, such as channel, Z- and multi-web sections. Experimental and analytical findings (Winter & Pian 1946, Rhodes & Nash 1998, Young & Hancock 2001) were employed to develop the empirical design rules in the early versions of the North American Specification (NAS) (2016) and Australian/New Zealand Standard (AS/NZS) (2005) for the design of cold-formed steel structures. In these design provisions, predictive formulae are provided for four isolated loading conditions, namely Interior-Two-Flange (ITF), End-Two-Flange (ETF), End-One-Flange (EOF) and Interior-One-Flange (IOF), as demonstrated in Fig. 1. Apart from the aforementioned investigations into the web crippling behaviour of open sections, research efforts have also been dedicated to tubular sections by Zhao and Hancock (1992), Zhou and Young (2006) and Li and Young (2018).

Structural instability phenomena are typically treated in international design standards through the use of strength curves, formulated on the basis of the normalised slenderness of the element. This has not, thusfar, been the case for web crippling design, but a number of studies by Natário et al. (2016, 2017) have been performed in this direction. The elastic buckling load for web crippling is inherently required within the calculation procedure, for which existing investigations are scarce. Natário et al. (2015) developed the software GBTWEB to obtain the elastic buckling load for web crippling as a convenient alternative to finite

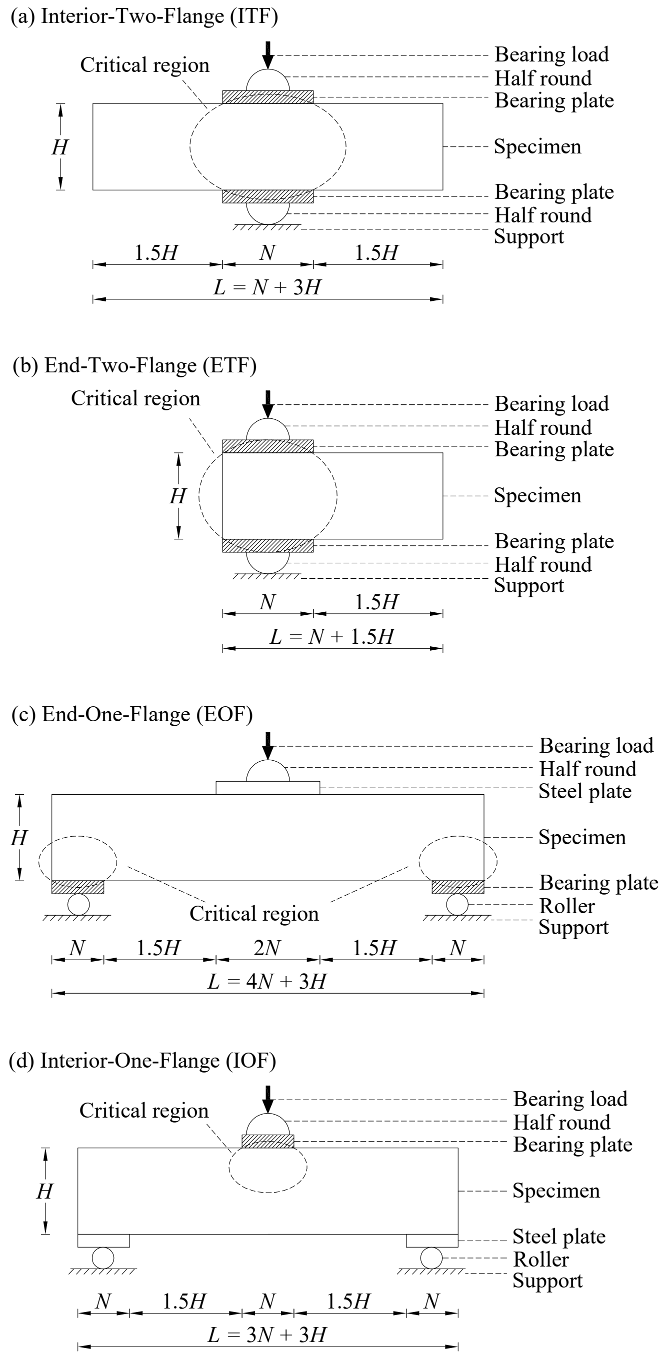

Figure 1: Demonstration of the (a) Interior-Two-Flange (ITF) (b) End-Two-Flange (ETF) (c) End-One-Flange (EOF) and (d) Interior-One-Flange (IOF) concentrated transverse loading conditions, as defined in the NAS and AS/NZS design specifications.

element (FE) modelling, which has been successfully employed in the strength prediction of web crippling failure using the DSM under ETF and ITF loading conditions (2016, 2017).

Hitherto, and to the best of the authors' knowledge, there has been no reported comprehensive investigation into the elastic buckling load for web crippling of tubular sections. Hence, the current study aims to bridge this research gap by developing formulae for predicting the elastic buckling load for web crippling of RHS and SHS profiles subjected to concentrated transverse forces. A detailed version of the present study is available (Dai et al. 2025) for reference.

2 GENERAL CONCEPT

2.1 *Concept*

The underlying concept for the approach presented herein is that the elastic buckling load for web crippling of RHS members, denoted as F_{cr}, is between a theoretical lower bound $F_{\mathrm{cr,lower}}$, where no adjacent region (beyond the bearing length) is mobilised, and a practical upper bound $F_{\mathrm{cr,upper}}$, where the adjacent region is mobilised to its maximum extent. This general concept is illustrated in Fig. 2.

The theoretical lower bound $F_{\mathrm{cr,lower}}$ is the elastic buckling load of a wide plate with cross-sectional dimensions $N \times t$ and length h_{w} with partially restrained boundary conditions along the loaded edges (arising from the rotational restraint afforded by the flanges) and free boundary conditions along the unloaded edges. A practical upper bound for the maximum influenced length, generally formulated as $N + nH$, is proposed based on FE analysis results for different loading conditions (i.e., $n = 2$ for ITF and $n = 0.5$ for ETF). Where the elastic buckling load for web crippling F_{cr} lies between these two bounds is expressed through the mobilisation coefficient ζ, which ranges from 0, for no mobilisation, to 1, for maximum mobilisation. Hence, the elastic buckling loads for web crippling of RHS members, denoted as $F_{\mathrm{cr},N_{\mathrm{eff}}}$ herein, can be expressed in the general form thus:

$$F_{\mathrm{cr},N_{\mathrm{eff}}} = F_{\mathrm{cr,lower}} + \zeta(F_{\mathrm{cr,upper}} - F_{\mathrm{cr,lower}}) \quad \text{where} \quad 0 \leq \zeta \leq 1. \quad (1)$$

Here, the lower bound of $\zeta = 0$ corresponds to $F_{\mathrm{cr},N_{\mathrm{eff}}} = F_{\mathrm{cr,lower}}$, which typically corresponds to the condition where a short structural member is fully loaded by the concentrated transverse force; the upper bound of $\zeta = 1$ corresponds to $F_{\mathrm{cr},N_{\mathrm{eff}}} = F_{\mathrm{cr,upper}}$, which occurs when the adjacent material is mobilised to its maximum extent for highly concentrated transverse forces in a sufficiently long structural member.

2.2 *General formulae*

The general formulae for determining the theoretical lower bound and the practical upper bound in Eq. (1) can be expressed in a general form thus:

$$F_{\mathrm{cr},\widetilde{N}} = \frac{\pi^2 E t^3 \widetilde{N}}{12(1-\nu^2)(\eta h_{\mathrm{w}})^2}. \quad (2)$$

Here, $\widetilde{N}$ is the generalised width, which is equal to N for the theoretical lower bound, N_{eff} for the target elastic buckling load for web crippling, $N + 2H$ for the practical upper bound under the ITF loading condition and $N + 0.5H$ for the practical upper bound under the ETF loading condition, while E is

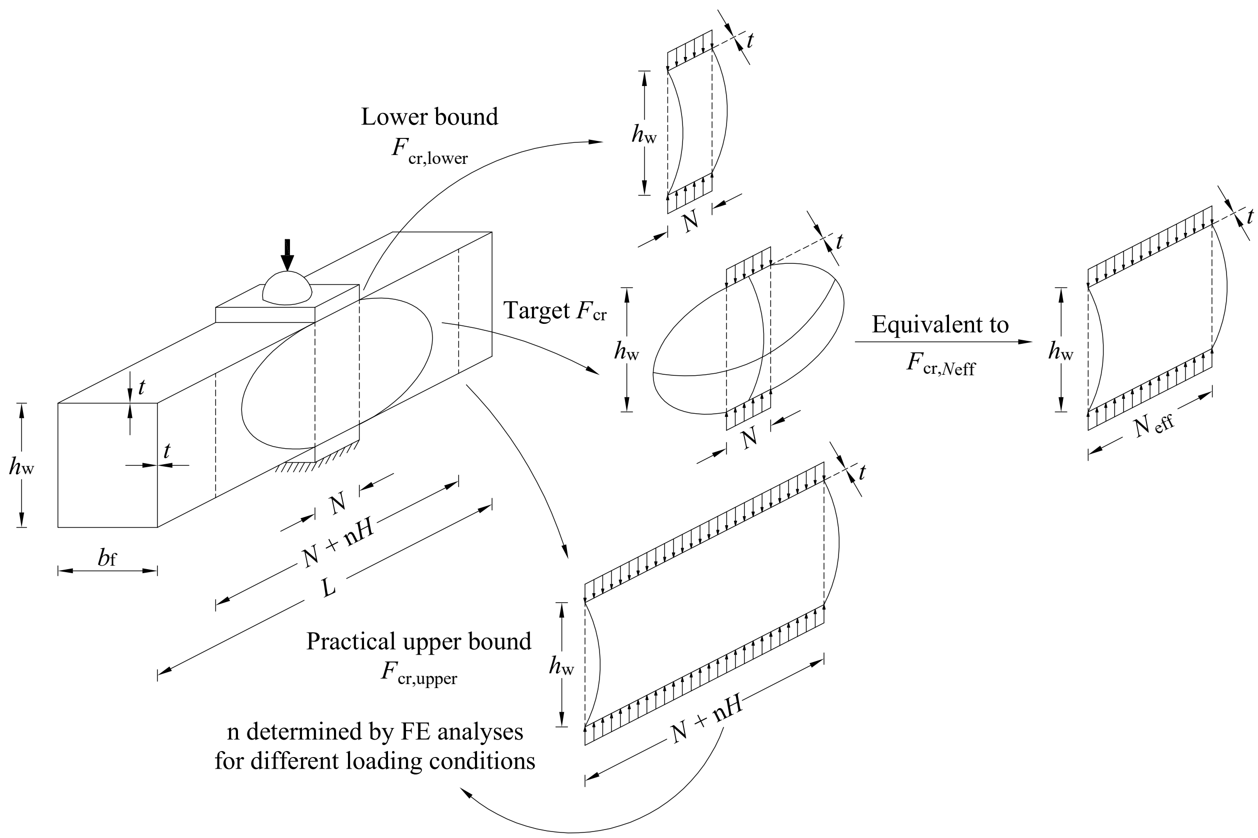

Figure 2: Illustration of the general concept of the lower and upper bounds to the elastic buckling load of an RHS under concentrated transverse loading.

the Young's modulus and ν is the Poisson's ratio of the material. The familiar $(1-\nu^2)$ term in the denominator accounts for the anticlastic plate bending being restrained due to plate continuity. The boundary conditions along the loaded edges are considered as partially restrained, which accounts for the influence of the bending stiffness of the flange on web buckling through the coefficient η. Formulae for η are developed based on numerical and analytical results.

3 NUMERICAL MODELLING

The 4-noded 'S4R' shell element (2016) was employed to model the RHS members. A general mesh size of approximately 5 mm was employed throughout the numerical modelling process, which typically resulted in at least 10 elements along each web and flange. A finer mesh size of approximately 2.5 mm was employed in the curved regions of the rounded corners and in the vicinity of the bearing loads and supports to capture the mechanical behaviour accurately. A Young's modulus $\mathrm{E} = 210,000\ \mathrm{N/mm^2}$ and a Poisson's ratio $\nu = 0.3$ were employed throughout the study; the proposed formulae do however apply to all isotropic materials. Centreline dimensions were considered throughout the presented calculations.

Instead of modelling the bearing and support plates explicitly, the loads transferred into the structural member are modelled herein through uniformly distributed load directly applied to the contacting nodes; these nodes should lie along the intersections between the flanges and the corner radii, and within the bearing and support plate lengths. With this modelling technique, the load eccentricity to the webs owing to the corner radii is also successfully reflected. The linear bifurcation analyses (LBA) were conducted with unit loads, so that the elastic critical buckling loads were directly linked to the output eigenvalues.

The boundary conditions employed in the FE models vary with different loading arrangements, and are determined such that the practical boundary conditions are reflected without over-constraints, and the merits of symmetry are utilised. The details of the boundary and loading conditions of the numerical models are presented by Dai et al. (2025).

A comprehensive parametric study was conducted, encompassing a broad spectrum of cross-sectional geometric proportions and bearing lengths across the four standard loading conditions, alongside their transitional cases. These ranges encompass the practical domain for engineering applications and the parametric domain studied in existing research work.

4 TWO-FLANGE (TF) LOADING

4.1 *Interior-Two-Flange (ITF) loading*

For the ITF loading condition, the lower bound $F_{\mathrm{cr},N}$ can be calculated using Eq. (2) with $\widetilde{N} = N$. The practical upper bound is determined as the maximum mobilised region obtained from the FE results. It is found that H on each side of the bearing force is adequate in practice within the studied domain, leading to a total of $N + 2H$ as the $\widetilde{N}$ in Eq. (2). The coefficient ζ for ITF loading can be back-calculated by rearranging Eq. (1), and using FE results $F_{\mathrm{cr,FE}}$ together with the calculated lower and upper bounds thus:

$$\zeta = \frac{F_{\mathrm{cr,FE}} - F_{\mathrm{cr},N}}{F_{\mathrm{cr},N+2H} - F_{\mathrm{cr},N}} = \frac{N_{\mathrm{eff,FE}} - N}{2H}$$

$$\text{where} \quad 0 \le \zeta \le 1. \quad (3)$$

The coefficient ζ can also be expressed in terms of lengths as presented in Eq. (3), which is easier to visualise. The relationship between ζ and N/H for the full parametric study under ITF loading condition is presented in Fig. 3. ζ is found to vary monotonically with H/B, so the two most extreme H/B ratios ($H/B = 0.4$ and $H/B = 0.25$) in the studied domain are selected as references, namely ζ_4 as the lower reference and $\zeta_{0.25}$ as the upper reference; polynomial expressions are developed for the two references thus:

$$\begin{aligned} \zeta_4 &= 0.045(N/H)^2 - 0.286N/H + 0.508, \\ \zeta_{0.25} &= 0.032(N/H)^2 - 0.207N/H + 0.800, \end{aligned} \quad (4)$$

which are shown to capture the FE results accurately.

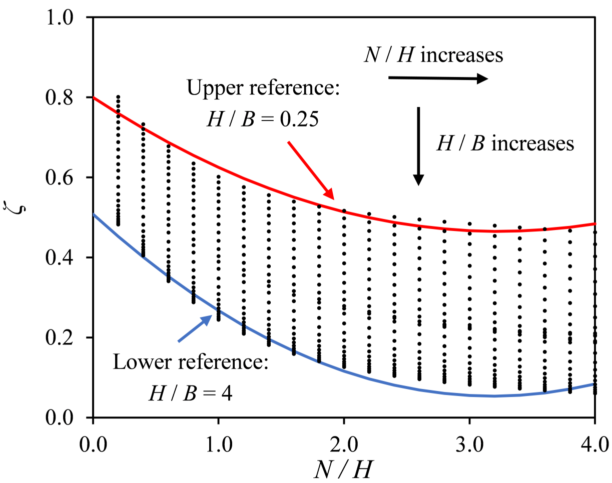

Figure 3: Relationship of ζ against N/H obtained from FE results alongside the proposed lower and upper references for ITF loading condition.

An auxiliary parameter Δ_{F} is introduced to quantify the position of a specific ζ value relative to its corresponding lower and upper references thus:

$$\Delta_{\mathrm{F}} = \frac{\zeta - \zeta_4}{\zeta_{0.25} - \zeta_4}. \quad (5)$$

The relationship between Δ_{F} and H/B obtained from FE results is plotted in Fig. 4; a function is developed which successfully captures the FE results thus:

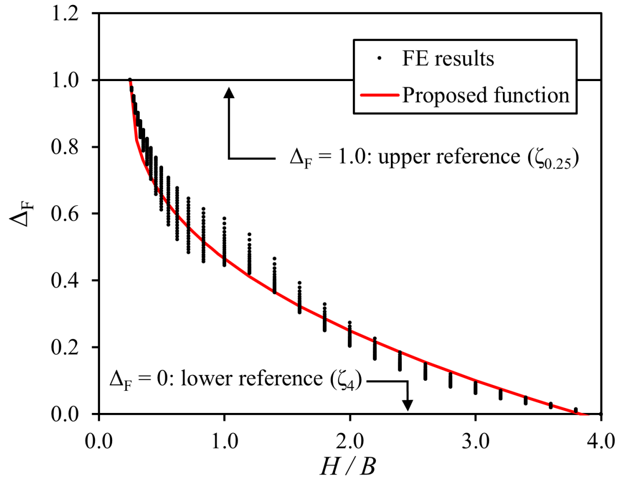

Figure 4: Parameter Δ_{F} obtained from FE results and proposed function against H/B for ITF loading condition.

$$\Delta_{\mathrm{F}} = 1 - 0.6(H/B - 0.25)^{0.4} \quad \text{but} \quad 0 \le \Delta_{\mathrm{F}} \le 1. \quad (6)$$

The elastic buckling loads for web crippling predicted using the proposed formulae are compared against the FE results, with a mean of 0.99 and a CoV of 0.02, which is judged to be accurate and slightly safe sided.

4.2 *End-Two-Flange (ETF) loading*

For the ETF loading condition, the lower bound remains the same as that for the ITF loading condition, whereas the maximum mobilised extent for the ETF loading condition obtained from the FE results is found to be $0.5H$, as opposed to H for ITF loading, leading to a total of $N + 0.5H$ as the $\widetilde{N}$ in Eq. (2).

The coefficient ζ for the ETF loading condition can be back-calculated by using Eq. (3) and substituting in the corresponding upper bound. Similar to the procedures described in Section 4.1, two references are selected at the extreme H/B ratios thus:

$$\begin{aligned} \zeta_4 &= 0.042(N/H)^2 - 0.271N/H + 0.450, \\ \zeta_{0.25} &= 0.021(N/H)^2 - 0.230N/H + 0.905. \end{aligned} \quad (7)$$

The auxiliary parameter Δ_{F}, as previously defined in Eq. (5), is determined for the ETF loading condition following similar procedures thus:

$$\Delta_{\mathrm{F}} = 1 - 0.65(H/B - 0.25)^{0.35} \text{ but } 0 \le \Delta_{\mathrm{F}} \le 1. \quad (8)$$

The elastic buckling loads predicted using the proposed formulae are compared against the FE results, with a mean of 0.99 and a CoV of 0.02, which is judged to be accurate and slightly conservative.

4.3 *Transition from ETF to ITF loading*

The transitional cases between the ETF and ITF loading conditions feature the clear distance from the edge of the bearing force to the free end, denoted as L_{e}, as illustrated in Fig. 5. The potential region that can be mobilised by the bearing force first increases sharply with this clear distance; this increase becomes more gradual as the case eventually converges to the ITF loading condition. The former pattern signifies the importance of the end clear distance on the increase in the elastic buckling load, whereas the latter pattern indicates a reduced and eventually negligible impact.

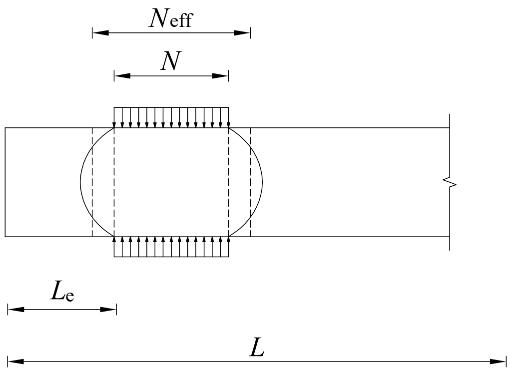

Figure 5: Demonstration of the transitional case between ETF and ITF loading conditions.

A cut-off point is therefore defined to pinpoint the threshold between these two distinct patterns. Functions describing this cut-off point are presented by Dai et al. (2025). For cases where the end clear distance is significant, the elastic buckling load $F_{\mathrm{cr,TF}}$ is approximated to vary linearly with length between the lower bound $F_{\mathrm{cr,ETF}}$ and the upper bound $F_{\mathrm{cr,ITF}}$. For cases where the end clear distance is insignificant, $F_{\mathrm{cr,TF}}$ is approximated as the same as that of its corresponding ITF loading condition $F_{\mathrm{cr,ITF}}$, since the difference is sufficiently small to be deemed as negligible.

The elastic buckling loads for web crippling predicted using the proposed formulae are compared against the FE results, with a mean of 0.99 and a CoV of 0.02, which is judged to be accurate and safe sided.

5 ONE-FLANGE (OF) LOADING

5.1 *Transition from ETF to EOF loading*

The transition between ETF and EOF loading conditions features the central distance between the bearing load and the support, denoted as L_{d}, as presented in Fig. 6. The critical region of failure under these loading conditions is expected to occur at the supports.

The most critical buckling mode is not always web crippling dominant, but can also be bending or shear dominant, owing to the inevitable coexisting bending and shear inherent within the loading setup. These coexisting bending moment and shear force, associated with the FE results for the applied concentrated forces $F_{\mathrm{cr,FE}}$, are denoted as $M_{\mathrm{cr,FE}}$ and $V_{\mathrm{cr,FE}}$, respectively. For reference purposes, the calculated elastic buckling moment of the full cross-sections subjected to bending (Gardner et al. 2019), denoted as $M_{\mathrm{cr,0}}$, and the calculated elastic shear buckling load

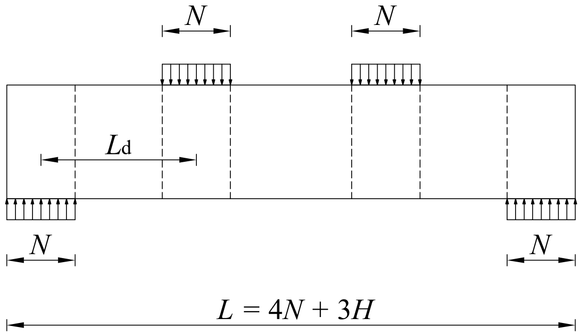

Figure 6: Illustration of the transitional case between ETF and EOF loading conditions.

(Timoshenko & Woinowsky-Krieger 1959), denoted as $V_{\mathrm{cr,0}}$, are obtained. The coexisting bending moment and shear force obtained from the FE results are normalised by their corresponding references, denoted as $M_{\mathrm{cr,FE}}/M_{\mathrm{cr,0}}$ and $V_{\mathrm{cr,FE}}/V_{\mathrm{cr,0}}$, respectively, to represent their relative contributions towards buckling.

Herein, the cases where web crippling is dominant or at least influential are determined by the criterion that $V_{\mathrm{cr,FE}}/V_{\mathrm{cr,0}} + M_{\mathrm{cr,FE}}/M_{\mathrm{cr,0}} \leq 1$, and are the focus of the present section. The expression for a general transition between the ETF and EOF loading conditions, denoted as $F_{\mathrm{cr,0,ETF\text{-}EOF}}$, is calibrated based on the FE results for these cases thus:

$$F_{\mathrm{cr,0,ETF\text{-}EOF}} = F_{\mathrm{cr,0,ETF}} \left[1.7/(1 + e^{-2L_{\mathrm{d}}/N}) + 0.15\right]. \quad (9)$$

The elastic buckling loads for web crippling predicted using the proposed formulae are compared against the FE results for cases where web crippling is critical, with a mean of 0.96 and a CoV of 0.05, which is judged to be accurate and safe sided.

The developed function in Eq. (9) has also been employed to predict the elastic buckling load when the web crippling mode is non-critical. A Python script was developed to interrogate the parametric FE results automatically and identify each first web crippling mode. A comparison of the predictions against the FE results over the full parametric study, including cases where web crippling is critical and non-critical, shows that the proposed function provides accurate and slightly conservative predictions. The detailed procedures are presented by Dai et al. (2025).

5.2 *Transition from ITF to IOF loading*

The transition between ITF and IOF loading conditions are split into two sub-categories: support expansion and support separation, featuring the central distance L_{d}, as illustrated in Fig. 7. The critical region of failure under these loading conditions is expected to occur at mid-span.

As in Section 5.1, the cases where web crippling is dominant are focused upon herein. The elastic buckling load for a general transition case between the ITF and IOF loading conditions $F_{\mathrm{cr,0,ITF\text{-}IOF}}$ can be deter-

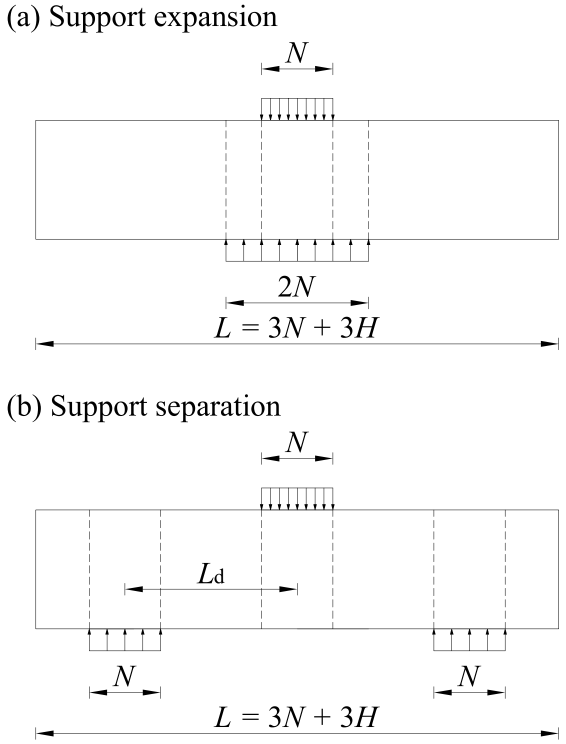

Figure 7: Illustration of the transitional cases with (a) support expansion and (b) support separation between ITF and IOF loading conditions.

mined thus:

$$F_{\text{cr,0,ITF-IOF}} = F_{\text{cr,0,ITF}}\left[1/(1+e^{-2.6L_{\text{d}}/H})+0.5\right]. \quad (10)$$

The elastic buckling loads for web crippling predicted using the proposed formulae are compared against the FE results, with a mean of 0.99 and a CoV of 0.04, which is judged to be accurate and safe sided.

As in Section 5.1, the developed function in Eq. (10) has also been employed to predict the elastic buckling load when the web crippling mode is non-critical. A comparison of the predictions against the FE results over the full parametric study shows that the developed function provides accurate and slightly conservative predictions.

6 CONCLUSIONS

Formulae for determining the elastic buckling loads for web crippling of structural steel RHS profiles under concentrated transverse forces were presented herein. It was found that the predicted elastic buckling load is bounded by a theoretical lower bound, where no adjacent material beyond the loaded length is mobilised, and a practical upper bound, where the adjacent material is mobilised to its maximum extent. These bounds can be expressed as the elastic buckling load of a wide plate with a length of the web depth and different widths. The level of mobilisation is accounted for through a coefficient ζ that ranges between 0, for no mobilisation, and 1, for maximum mobilisation. The rotational stiffness afforded to the webs by the flanges is also captured. Formulae for calculating the elastic buckling loads for web crippling under the four codified loading scenarios in the NAS and AS/NZS, namely the ITF, ETF, IOF and EOF loading conditions, alongside their transitional cases, were developed. The formulae were calibrated using results from FE analyses conducted within the commercial package ABAQUS. RHS profiles with a broad spectrum of cross-sectional geometric proportions and bearing lengths encompassing the aforementioned loading conditions were considered. The developed formulae provide accurate predictions that are typically within 5% of the numerical values. The developed formulae can be employed as a convenient alternative to numerical methods within structural design frameworks based on the full section normalised slenderness, e.g., DSM and CSM.

REFERENCES

ABAQUS (2016). *Version 6.16 Analysis User's Guide*. Dassault Systemes Simulia Corporation, Providence, RI, USA.

Australian/New Zealand Standard (AS/NZS) (2005). *Cold-formed steel structures, AS/NZS 4600*. Standards Australia, Sydney, Australia and Standards New Zealand, Wellington, New Zealand.

Dai, R., L. Gardner, & M. A. Wadee (2025). Formulae for calculating elastic buckling loads of rectangular hollow sections under concentrated transverse forces. *Thin-Walled Structures* ***, ******.

Gardner, L., A. Fieber, & L. Macorini (2019). Formulae for calculating elastic local buckling stresses of full structural cross-sections. *Structures 17*, 2–20.

Li, H.-T. & B. Young (2018). Design of cold-formed high strength steel tubular sections undergoing web crippling. *Thin-Walled Structures 133*, 192–205.

Natário, P., N. Silvestre, & D. Camotim (2015). *GBTWEB, GBT-based code for web buckling analysis of members under localised loads*. freely available at: http://www.civil.ist.utl.pt/gbtweb/.

Natário, P., N. Silvestre, & D. Camotim (2016). Direct strength prediction of web crippling failure of beams under ETF loading. *Thin-Walled Structures 98*, 360–374.

Natário, P., N. Silvestre, & D. Camotim (2017). Web crippling of beams under ITF loading: A novel DSM-based design approach. *Journal of Constructional Steel Research 128*, 812–824.

North American Specification (NAS) (2016). *North American Specification for the design of cold-formed steel structural members, AISI S100-16*. American Iron and Steel Institute (AISI), Washington D.C., USA.

Rhodes, J. & D. Nash (1998). An investigation of web crushing behaviour in thin-walled beams. *Thin-Walled Structures 32*(1-3), 207–230.

Timoshenko, S. & S. Woinowsky-Krieger (1959). Theory of plates and shells: Bending moments in a simply supported rectangular plate with a concentrated load. Technical report.

Winter, G. & R. H. J. Pian (1946). *Crushing strength of thin steel webs*. Cornell University.

Young, B. & G. J. Hancock (2001). Design of cold-formed channels subjected to web crippling. *Journal of Structural Engineering 127*(10), 1137–1144.

Zhao, X.-L. & G. J. Hancock (1992). Square and rectangular hollow sections subject to combined actions. *Journal of Structural Engineering 118*(3), 648–667.

Zhou, F. & B. Young (2006). Cold-formed stainless steel sections subjected to web crippling. *Journal of Structural Engineering 132*(1), 134–144.